

## Deliverable 3.1 Synthesis of advanced active materials

Manuel J. Pinzón (CIC), Roman Mysyk (CIC), Jon Serrano (CIC), Daniel Carriazo (CIC)

Dick Van De Kleut (BYD), Obinna Egwu Eleri (BYD)

Andrea Hainthaler (FSU), Andrea Balducci (FSU)

Juan Pablo Badillo (ELYTE)

Thierry Brousse (IMN)

Hugo Mazoyer (IRT-JV)



*Funded by the European Union. Views and opinions expressed are however those of the author(s) only and do not necessarily reflect those of the European Union or Horizon Europe. Neither the European Union nor the granting authority can be held responsible for them. No 101092080*

<b>Deliverable No.</b>	MUSIC D3.1	
<b>Related WP</b>	WP3	
<b>Deliverable Title</b>	Synthesis of advanced active materials	
<b>Deliverable Date</b>	2025/09/22	
<b>Deliverable Type</b>	REPORT	
<b>Dissemination level</b>	Public (PU)	
<b>Written By</b>	Manuel Pinzón (CIC), Roman Mysyk (CIC), Jon Serrano (CIC), Daniel Carriazo (CIC), Dick Van De Kleut (BYD), Obinna Egwu Eleri (BYD), Andrea Hainthaler (FSU), Andrea Balducci (FSU), Juan Pablo Badillo (ELYTE), Thierry Brousse (IMN), Hugo Mazoyer (IRT-JV)	2025-08-26
<b>Checked by</b>	Andrea Balducci (FSU)	2025-09-04
<b>Reviewed by (if applicable)</b>	Andrea Hainthaler (FSU) Pierre-Louis Taberna (UPS)	2025-09-04
<b>Approved by</b>	Jon Ajuria (CIC) Elena Dosal (CIC)	2025-09-05 2025-09-22
<b>Status</b>	Final	2025-09-22

## Disclaimer / Acknowledgment



Copyright ©, all rights reserved. This document or any part thereof may not be made public or disclosed, copied or otherwise reproduced or used in any form or by any means, without prior permission in writing from the MUSIC Consortium. Neither the MUSIC Consortium nor any of its members, their officers, employees or agents shall be liable or responsible, in negligence or otherwise, for any loss, damage or expense whatever sustained by any person as a result of the use, in any manner or form, of any knowledge, information or data contained in this document, or due to any inaccuracy, omission or error therein contained.

All Intellectual Property Rights, know-how and information provided by and/or arising from this document, such as designs, documentation, as well as preparatory material in that regard, is and shall remain the exclusive property of the MUSIC Consortium and any of its members or its licensors. Nothing contained in this document shall give, or shall be construed as giving, any right, title, ownership, interest, license or any other right in or to any IP, know-how and information.

This project has received funding from the European Union's Horizon Europe programme for research and innovation under grant agreement No. 101092080. This document reflects the views of the author and does not reflect the views of the European Commission. While every effort has been made to ensure the accuracy and completeness of this document, the European Commission cannot be held responsible for errors or omissions, whatever their cause.

## Publishable summary

The MUSIC project aims to develop a sodium-ion capacitor (SIC), which can provide more power than a conventional lithium-ion battery but at the same time has a higher energy density than a supercapacitor. To achieve that outstanding target, a strong effort is devoted to the development of new active materials and components that show improved performance when integrated in SICs.

As part of D3.1, BYD worked on the synthesis of activated carbons and benchmarking of commercially available activated carbons to be used as positive electrodes for Na-ion hybrid capacitors. CIC focused on the synthesis of advanced hard and soft carbons from different precursors (biowastes, synthetic and recycled polymers) and the surface modifications of commercially available activated carbons to improve both their textural properties and voltage stability window. Simultaneously, JVI and CNRS-IMN focused on the carbon fibers recycled from the aeronautic industry. Further, FSU and ELY developed different electrolyte formulations that outperform the reference electrolytes used for this technology.

# Table of Contents

1	Introduction .....	7
2	Methods and Results .....	8
2.1	Advanced Electrode Materials .....	8
2.1.1	Advanced high specific surface carbons .....	8
2.1.2	Advanced carbon materials as anode for high power sodium storage .....	14
2.2	Advanced Electrolytes .....	25
3	Discussion and Conclusions .....	28
3.1	Advanced Electrode materials .....	28
3.1.1	Modified High Specific Surface Area Activated Carbons .....	28
3.1.2	Soft carbon from PVC precursors .....	28
3.1.3	Hard carbons .....	28
3.1.4	Recycled CNFs.....	29
3.2	Advanced Electrolytes .....	30
4	Recommendation .....	31
5	Risk register .....	31
6	Acknowledgement .....	32

## List of Figures

Figure 1. Moisture and ash content of wood samples (a) powders, fibres and chips and (b) Sawdust. .	9
Figure 2. (a) Cumulative SSA and (b) pore size distribution of the reference sample YP80F and the HNO <sub>3</sub> treated one. ....	13
Figure 3. a) SEM images comparison of PVC-derived SC without and with an intermediate ball milling step, b) XRD pattern of the PVC derived soft carbon and c) average charge capacity of the PVC-derived soft carbon. ....	15
Figure 4. Hard carbons derived from Biowaste: Scanning electron microscopy (SEM) images at 2500x magnification, (a) OP ,(b) OP_X (inset: 12000x mag), (c) OP_X_4BM (inset: 25000x mag) and (d) OP_X_1BM (inset: 25000x mag). (e) CNT at 12000x mag (inset: 63000x mag). (f) Raman spectra of the different HC's and CNT's. ....	16
Figure 5. Biowaste derived Hard carbons: Charge-Discharge profiles at different C-rates. Electrochemical performance, (middle up) Coulombic efficiency and (middle down) Rate capability. .	19
Figure 6. Hard carbons derived from Xylose: Scanning electron microscopy (SEM) images at 2000x magnification (inset: 32000x magnification), (a) Xyl 1 ,(b) Xyl 2 and (c) Xyl 3. Charge-Discharge profiles at different C-rates, (d) Xyl 1 ,(e) Xyl 2 and (f) Xyl 3. Electrochemical performance, (g) Coulombic efficiency and (h) Rate capability. ....	21
Figure 7. a) Raman Spectra of PAN and Pitch-based carbon fibers recycled by different recycling processes and the ratio of the amorphous and graphitic carbon in the carbon fibers; b) particle size distribution of PAN-based carbon fibers recycled by vapothermolys after different ball-milling times; c) specific surface vs milling time at 400 rpm for PAN carbon fibers recycled by vapothermolysis; d) electrode surface for a 1 hour ball-milling time of PAN-based carbon fibers recycled by vapothermolysis. ....	23
Figure 8. Discharge-charge profiles at 50 mA.g <sup>-1</sup> of PAN carbon fibers recycled by vapothermolysis a) milled 2h and b) milled 4h; c) specific charge/discharge capacity vs current density for different PAN-based carbon fibers recycled with vapothermolysis and pyrolysis processes, compared to standard hard carbon negative electrode (HC, black plot); d) specific capacity vs discharge time for different PAN-based carbon fibers recycled with vapothermolysis and pyrolysis processes, compared to standard hard carbon negative electrode. ....	24

## List of Tables

Table 1. Comparison of the properties of the reference AC and modified AC. ....	10
Table 2. Performance comparison of SAC samples produced using procedure 2. ....	11
Table 3. Textural properties of the commercial samples. ....	12
Table 4. Electrochemical performance analysis of the commercial samples. ....	12
Table 5. XPS atomic composition of pristine and HNO <sub>3</sub> -treated activated carbon YP-80F. ....	14
Table 6. Characteristics of hard carbons derived from biowaste. ....	20
Table 7. Features of some hard carbons derived from xylose. ....	22
Table 8. Electrolyte formulations provided by E-lyte to different partners. ....	26
Table 9. Conductivity values of selected electrolyte formulations measured by E-lyte. ....	27
Table 10. Risk Register. ....	31
Table 11. Project Partners. ....	32
Table 12. Quality Assurance. ....	<b>Error! Bookmark not defined.</b>

## List of Equations

No entries for the list of equations found.

## Abbreviations

SYMBOL	SHORTNAME
t	Time

# 1 Introduction

The main objective of the MUSIC project is the development of a sodium-based hybrid supercapacitor that fulfils different target specifications such as high energy density, long cycle life, low cost, and sustainability, and its validation at laboratory and prototype scale.

To achieve this, the strategy initially relied on the use of commercially available materials for the different cell components. In parallel, Work Package 3 (WP3) focuses on the development of advanced alternative materials with improved properties to replace the benchmarking ones and thereby improve the overall full cell performance.

The novel materials developed in the first part of the project include hard carbons from different types of precursors, the use of carbon fibers from wastes, surface treated activated carbons, and advanced electrolytes. These materials have been developed following different synthetic strategies to tune their properties and, thus, improve their electrochemical performance as sodium-ion hybrid capacitor components.

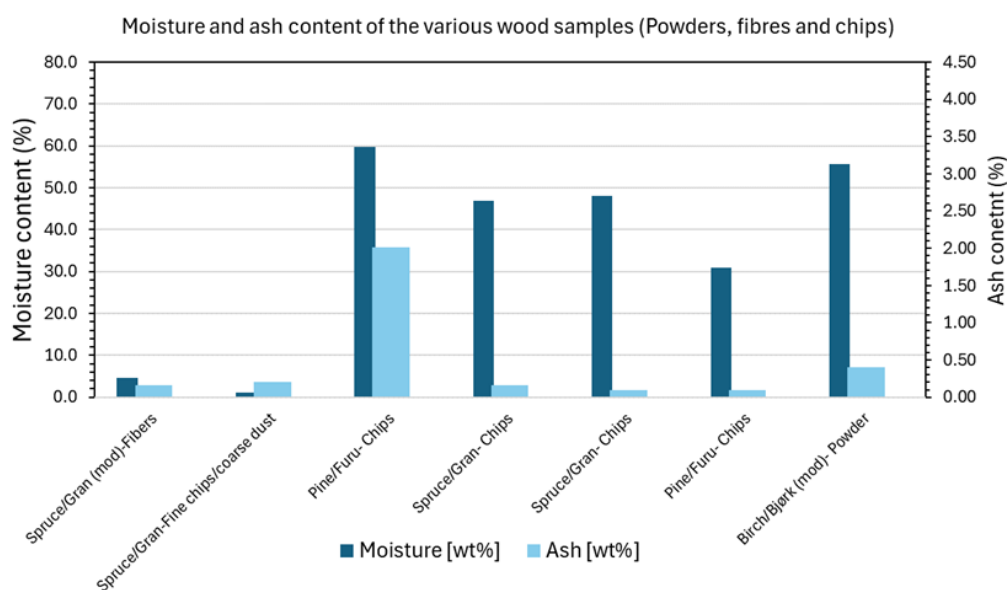
This deliverable presents some of the most interesting and representative results obtained from each of these components, including preparation routes, physicochemical characterization, and, in some cases, electrochemical evaluation. The most promising materials are identified based on their individual performance and are proposed for further investigation in future stages through the combination of several of them.

## 2 Methods and Results

### 2.1 Advanced Electrode Materials

#### 2.1.1 Advanced high specific surface carbons

Before the synthesis of super-activated carbons, a comprehensive examination of various wood samples sourced from six local wood mills in Norway was conducted. In total, 30 wood samples were obtained and classified into three types and particle shape (dust, fibres, chips, fine chips). Bulk density, moisture and ash content analysis were conducted on the samples using internal benchmarking processes. Analyzing these parameters was vital for the optimum characterization of the effect of activation conditions on the final produced AC since the moisture and ash content severely impacted the efficacy of the activation agent. Moreover, the moisture absorbency of these wood samples was also monitored after drying for a specific period to standardize the control method and highlight the effect of exposure to the ambient environment prior to activation. Figures 1 a and b show the different wood samples and the obtained moisture and ash content.





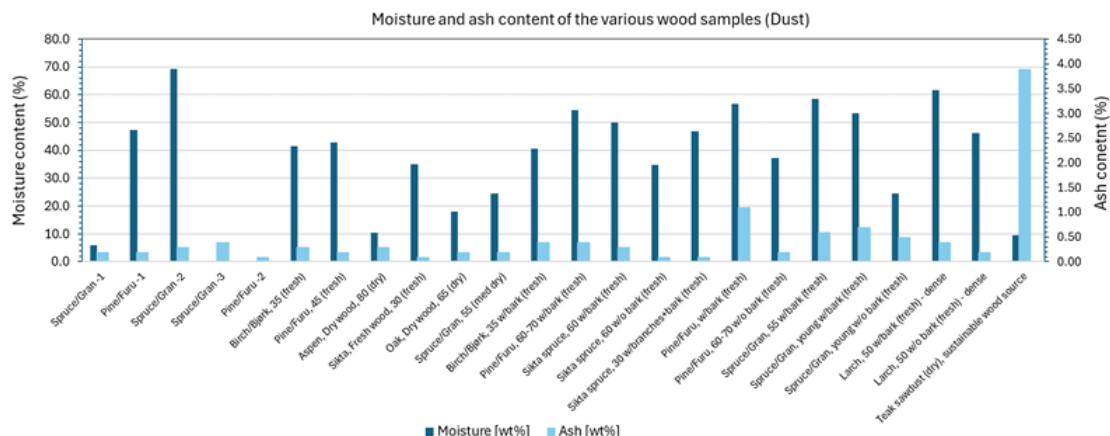


**Figure 1.** Moisture and ash content of wood samples (a) powders, fibres and chips and (b) Sawdust.

Sawdust samples from Spruce/Gran -1 (from supplier A) were the best samples with the criteria of low moisture content and ash content. However, ACs were prepared from the other samples using *Procedure 2* (explained below), and in the process, producing a comprehensive compilation of ACs and the effect of activation conditions on properties such as surface area, pore volume, electrode density, gravimetric and volumetric capacitance and self-discharge.

#### 2.1.1.1 Description of activation procedures

The initially developed activation procedure (*Procedure 1*) consisted of chemical activation, using a strong basic chemical activation agent and a metal additive incorporated to act as an oxygen scavenger during the activation process. The activation process was conducted in a horizontal tubular furnace at varying temperatures from 600 - 850 °C while incorporating a pre-carbonization step. A post-treatment acid-washing step was included to remove the metal additive and remnant activation agent. ACs synthesized using this method had surface areas up to 3000 m<sup>2</sup>/g and narrow pore size distribution. Moreover, the micropore volume increased as the additive content increased, while the mesopores decreased. Thus, enabling higher electrode densities.

A comparable AC synthesized without the metal additive also had a surface area of up to 3000 m<sup>2</sup>/g, though with extensive mesopores, which impacted the electrode density. In summary, the metal additive in the activation process modified the activation procedure, as well as the resulting surface and pore properties of the AC sample. The electrochemical performance of the AC produced with the metal additive (NDA) and without the additive (REF) was evaluated using CR2032 coin cells and the electrolyte 1 M TEABF<sub>4</sub> in PC. A summary of the compared performance is shown in Table 1.

**Table 1.** Comparison of the properties of the reference AC and modified AC.

S/N	Properties	REF	NDA	SAC
1	Surface area (m <sup>2</sup> /g)	3083	2924	2746
2	Pore volume (cm <sup>3</sup> /g)	1.884	1.522	1.57
3	Electrode density (g/cm <sup>3</sup> )	0.440	0.522	0.49
4	Specific capacitance (F/g) @ 0.1 A/g and 5 A/g	150/125	160/139	135/128
5	Volumetric capacitance (F/cm <sup>3</sup> ) @ 0.1 A/g and 5 A/g	66/55	84/73	66/63

Challenges faced in upscaling the AC (NDA) produced by *Procedure 1* due to the corrosive nature of the activation agent and flow problems encountered during continuous production using a rotary kiln. Therefore, a new activation procedure (*Procedure 2*) was developed that replaced the previously strong basic activation agent with phosphoric acid. The new activation procedure consisted of a two-step activation process involving a chemical activation step with the phosphoric acid and a physical activation step. After the activation process, a post-treatment washing step was also incorporated to purify the synthesized AC. The initial activation process conditions were developed using a horizontal tubular batch furnace with an AC yield between 1-5 g and successfully upscaled to 500 g using a rotary kiln. The properties of one of the best samples (SAC) produced using *procedure 2* is also compared in Table 1. Although SAC had much lower performance than the previous method, it remained the most feasible to upscale, with comparable performance to other commercially available AC.

Several research activities involving varying degrees of activation conditions were undertaken to increase the electrode density and volumetric performance to match commercial standards (specifically YEC-B). It was revealed that increasing the electrode density inversely affected the surface area and obtainable specific capacitance. Some selected samples are presented in Table 2.

**Table 2.** Performance comparison of SAC samples produced using procedure 2.

Sample ID	BET SA (m <sup>2</sup> /g)	Pore Volume D < 2 nm (cm <sup>3</sup> /g)	Pore volume D < 50 nm (cm <sup>3</sup> /g)	Specific capacitance (F/g @ 0.1 A/g)	Specific capacitance (F/g @ 5 A/g)	Rate capability (%)	Self-discharge (%)	Press density (g /cm <sup>3</sup> )	Volumetric Capacitance (F/cm <sup>3</sup> @ 0.1 A/g)	Volumetric Capacitance (F/cm <sup>3</sup> @ 5 A/g)
SAC22-014	1395	0.48	0.65	104.5	92.9	89	21	1	71	63
SAC22-015	1554	0.52	0.75	96.6	86.1	89	37	1	69	61
SAC21-025	2540	0.69	1.42	106.7	101.9	95	40	0.52	56	53
SAC21-026	2826	0.81	1.45	115.8	111.9	97	29	0.46	53	51
SAC21-027	2603	0.78	1.28	123.4	118.4	96	19	0.42	52	50
SAC21-032	2399	0.74	1.19	125.3	119.6	96	21	0.49	61	59
SAC21-033	2362	0.75	1.14	121.8	114.2	94	25	0.49	60	56
SAC21-034	2273	0.74	1.09	126.1	120.1	95	32	0.53	67	64
SAC21-036	2544	0.53	1.77	108.8	101.9	94	29	0.36	39	37
SAC21-037	2011	0.68	0.94	113.1	106.8	94	20	0.56	63	60
SAC21-038	2746	0.69	1.57	135.0	127.5	94	24	0.49	66	62
SAC21-039	2562	0.73	1.28	134.0	106.5	79	30	0.48	64	51

#### 2.1.1.2 Performance Benchmarking of commercially sourced activated carbons (AC)

Several commercially sourced activated carbon samples were used to select a suitable replacement after the issues encountered with upscaling the in-house produced AC. The commercial AC and their sources are listed below:

1. YEC-8B sourced from Fuzhou Yihuan Carbon Co., Ltd, China.
2. YP-80F sourced from Kuraray, Japan.
3. BAC sourced from BTR Corp, China
4. HCE202 sourced from Haycarb, Sri Lanka.

The textural properties of the samples were characterized using Nitrogen physisorption analysis; the results are presented in Table 3.

**Table 3.** Textural properties of the commercial samples.

Sample	BET Surface area (m <sup>2</sup> /g)	Total Pore* volume (cm <sup>3</sup> /g)	Micro pores* volume (cm <sup>3</sup> /g)	Mesopore * volume (cm <sup>3</sup> /g)	Particle density (g/cm <sup>3</sup> )
<b>YEC-8B</b>	1778	0.77	0.71	0.05	0.83
<b>YP-80F</b>	2274	1.07	0.77	0.29	0.66
<b>BAC</b>	1833	0.73	0.67	0.06	0.86
<b>HCE202</b>	1892	0.78	0.66	0.11	0.82

For the electrochemical performance analysis, electrodes were fabricated from the AC samples using the recipe 92% AC:8% PTFE and aided by a hot rolling press. CR20232 coin cells were assembled with electrode discs and 1M TEABF<sub>4</sub> in PC electrolyte. The electrochemical measurements were conducted in the potential window 1.25 to 2.5V, while the self-discharge was measured over 72 h after charging to 2.5 V. The results from the electrochemical performance analysis are presented in Table 4.

**Table 4.** Electrochemical performance analysis of the commercial samples.

Sample	Specific capacitance (F/g) @ 0.1mA	Press density (g/cm <sup>3</sup> )	Volumetric capacitance (F/cm <sup>3</sup> ) @ 0.1mA	Self-discharge rate (%)
<b>YEC-8B</b>	140	0.64	89	14
<b>YP-80F</b>	124	0.50	62	15
<b>BAC</b>	120	0.64	77	13
<b>HCE202</b>	108	0.69	74	10

To improve the performance of the positive electrode active material, commercially available YP80F activated carbon were treated with strong oxidant to increase specific surface area and tune porosity and improve voltage stability window to be more oxidation resistant.

The treatment of the activated carbon, whose behavior is most suitable for coupling with sodium electrolytes, is carried out in the following way:

Five hundred milligrams of activated carbon were treated with 10 mL of 10M  $\text{HNO}_3$  in an Erlenmeyer flask. Then it was stirred at 80 °C for 2 h. The resulting material is thoroughly washed with water until a neutral pH is reached, and dry in a oven overnight. The textual properties of the treated YP80F are also studied by plotting the SSA versus pore size (Figure 2a) and the differential pore volume *versus* pore size (Figure 2b) using the 2D-NLDFT method.

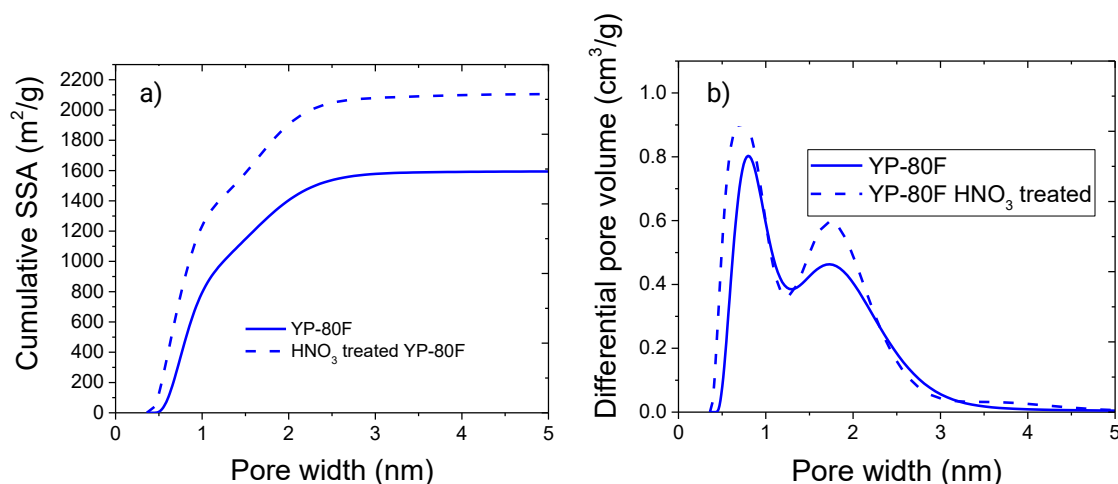


**Figure 2.** (a) Cumulative SSA and (b) pore size distribution of the reference sample YP80F and the  $\text{HNO}_3$  treated one.

It is observed that YP80F experiences an increase in its cumulative SSA after treatment, reaching SSA values of ca. 2150  $\text{m}^2/\text{g}$  and 2682  $\text{m}^2/\text{g}$  according to the 2D-NLDFT and BET methods, respectively. This treatment leads to an increase in strength, which can be explained using the pore size distribution (Figure 2). This figure shows that the additional pores are narrower than those of the initial material, so they may already be similar to or smaller than the size of the ion, thus generating steric hindrance to ionic transport. After the oxidation treatment applied to the YP80F, an interesting aspect is observed regarding the pores present in the material. The graphic representation of these pores, as shown in Figure 2b, reveals a notable increase in the narrowest pores. This increase is mainly concentrated in the micropores, those with a diameter between 0.5 nm and 2 nm. On the other hand, mesopores show a behavior quite similar to that of untreated carbon, suggesting that the treatment does not significantly affect this pore fraction.

The XPS analysis (Table 5) shows that the treatment of commercial carbon YP-80F with nitric acid does not significantly enrich the material with nitrogen but does so with oxygen.

**Table 5.** XPS atomic composition of pristine and HNO<sub>3</sub>-treated activated carbon YP-80F.

Element	Atomic composition, at %	
	YP-80F Atomic %	YP-80F, HNO <sub>3</sub> -treated Atomic %
C	94	84
N	-	1.2
O	5	15

## 2.1.2 Advanced carbon materials as anode for high power sodium storage

### 2.1.2.1 Soft carbon from PVC precursors

Recycling Polyvinyl Chloride (PVC) waste into functional carbon materials is strongly supported by EU policies like the Green Deal and Circular Economy Action Plan, which promote waste reduction and plastics reuse. Converting PVC into carbon for energy storage both reduces environmental impact and supports the shift to clean energy.

Soft carbon can outperform hard carbon in terms of rate capability, especially when the particle size is reduced. Particle sizes below 5  $\mu\text{m}$  are typically targeted to enhance sodium-ion diffusion and improve high-rate performance. However, the final particle size of the carbon strongly depends on the precursor and the processing route. While ball milling is a common method to reduce particle size, applying it to the final carbonized material can significantly damage the surface structure. This often leads to increased surface area, higher defect density, and consequently a higher initial Coulombic efficiency (ICE) loss due to excessive electrolyte decomposition.

To address this, the proposed strategy consists of three sequential steps. First, the precursor undergoes a low-temperature calcination at 500  $^{\circ}\text{C}$  to initiate partial carbonization and facilitate further processing. Second, the carbonized material is subjected to ball milling to reduce particle size. Finally, the milled powder is pyrolyzed at 800  $^{\circ}\text{C}$  to complete the carbonization process, yielding soft carbon with optimized particle size and minimized damaged surface. Figure 3a shows the effect of the ball milling, reducing the average particle size from 20 to 2  $\mu\text{m}$ . The XRD pattern of the ball milled SC (Figure 3b) show pure soft carbon material. The resulting soft carbon (Figure 3c) shows a ICE of 75.5% and first charge capacity of 214 mAh/g at C/15 rate, retaining 165 mAh/g at 1C and 93 mAh/g at 10C (1C = 372 mA/g).

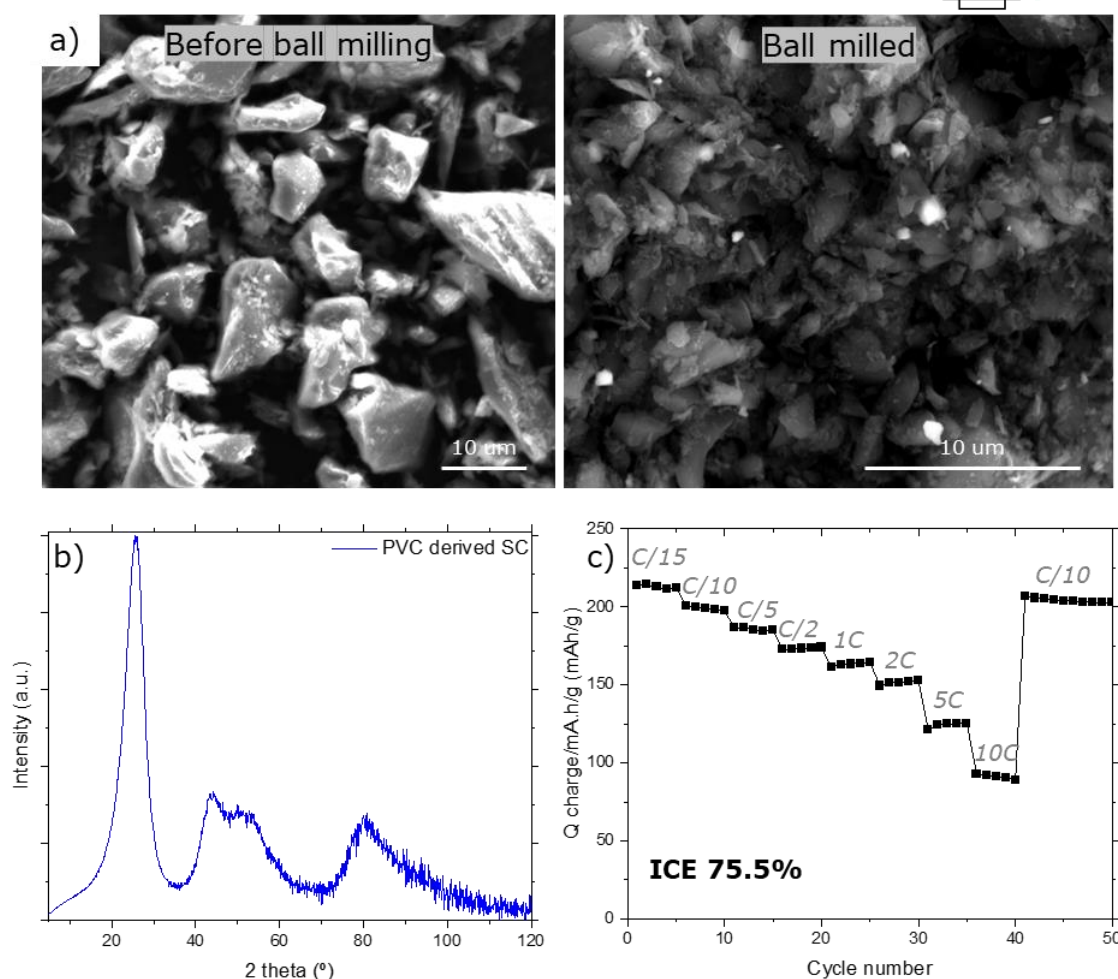


**Figure 3.** a) SEM images comparison of PVC-derived SC without and with an intermediate ball milling step, b) XRD pattern of the PVC derived soft carbon and c) average charge capacity of the PVC-derived soft carbon.

#### 2.1.2.2 Hard Carbons

The shift towards renewable energy necessitates the development of scalable, cost-efficient, and sustainable energy storage systems capable of operating efficiently at high power. Among the emerging technologies, sodium-ion capacitors (SICs) present a promising solution, merging the rapid charge/discharge characteristics of capacitors with the superior energy density typical of battery-type devices. A crucial component of SIC systems is the negative electrode, where hard carbon (HC) has emerged as the benchmark material. HC's highly disordered, turbostratic structure provides a distinctive combination of micropores, slit-like voids, and graphitic nanodomains, which together facilitate efficient sodium-ion storage. These structural features, in conjunction with HC's mechanical strength and chemical stability, make it an ideal material for high-power, long-cycle-life applications. Furthermore, HC's properties can be finely tuned through the selection of precursors and by adjusting chemical or thermal treatment conditions, enabling



optimization to meet specific electrochemical performance criteria. The key challenges associated with the synthesis and validation of HC negative electrodes derived from olive pits, a readily available waste material, are addressed in this part of the work package. Our goal is to enhance both the structural and morphological characteristics of HC to achieve competitive performance under high current densities.

**Biowaste derived HC's:** Initially, the olive pits were subjected to drying and crushing to obtain particles with a moderate level of homogeneity (c.a. 35-55  $\mu\text{m}$ ). The first approach involved applying a carbonization protocol in an inert nitrogen atmosphere ( $\text{N}_2$ , 500 mL/min) to the particulate material.

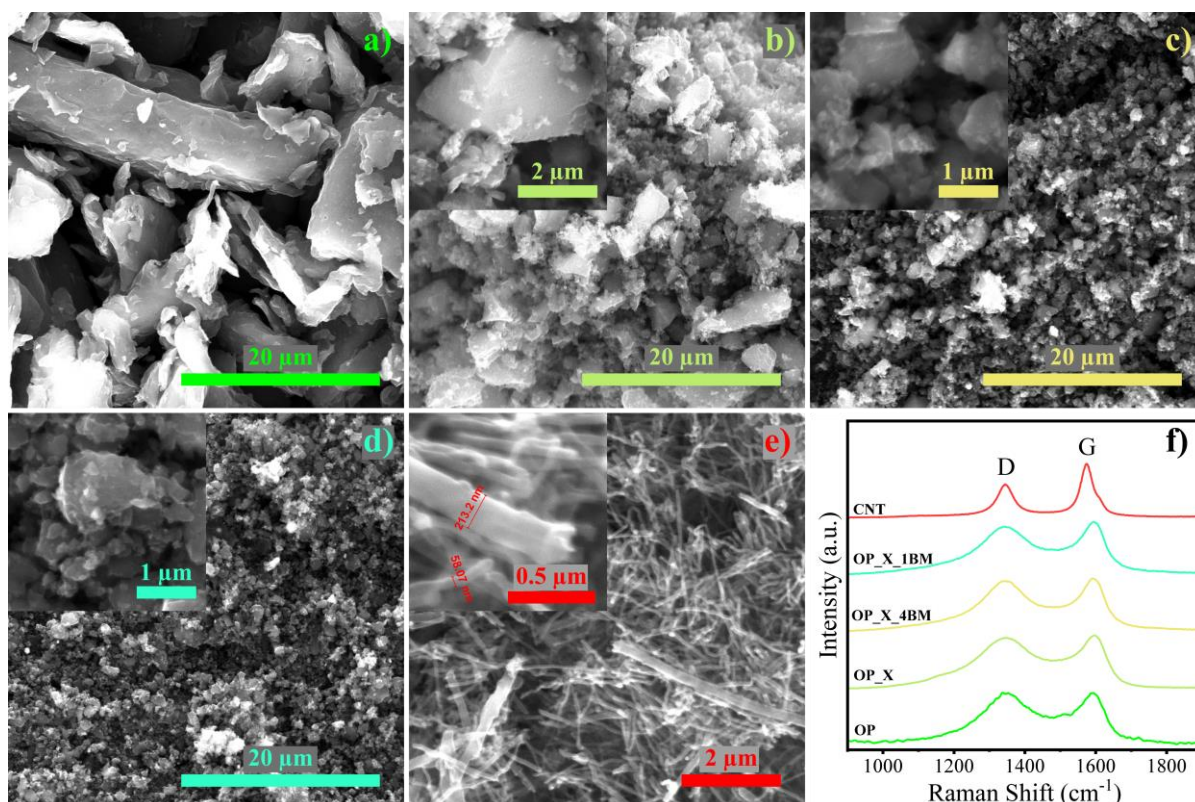


**Figure 4.** Hard carbons derived from Biowaste: Scanning electron microscopy (SEM) images at 2500x magnification, (a) OP, (b) OP\_X (inset: 12000x mag), (c) OP\_X\_4BM (inset: 25000x mag) and (d) OP\_X\_1BM (inset: 25000x mag). (e) CNT at 12000x mag (inset: 63000x mag). (f) Raman spectra of the different HC's and CNT's.

Protocol was carried out in three stages: 1. The temperature was increased from room temperature to 120°C at a rate of 10°C/min, followed by a 30-minute hold. 2. The temperature was then raised from 120°C to 500°C at a rate of 0.5°C/min and maintained at 500°C for 30 minutes. 3. Finally, the temperature was increased from 500°C to 1050°C at a rate of 10°C/min, and the material was held at the target temperature for 12 hours (sample OP). Figure 4a present scanning electron microscope (SEM) micrograph of the carbon material obtained following this carbonization process.



To improve the high C-rate performance of hard carbons (HCs), the precursor underwent a hydrothermal pretreatment prior to carbonization. Ground olive pits were mixed with an equal-volume solution of HCl and deionized water (1 mg powder per 2 mL acid) in a sealed autoclave, heated at  $5\text{ }^{\circ}\text{C}\cdot\text{min}^{-1}$  to  $105\text{ }^{\circ}\text{C}$ , and held for 6 h. The product was washed to neutral pH, filtered, and vacuum-dried at  $120\text{ }^{\circ}\text{C}$  overnight before carbonization following the previously described protocol (sample OP\_X\_4\_C). Figure 4b present SEM micrograph of the carbon material obtained following this acid pretreatment and carbonization process.

As the first alternative strategy to enhance the performance of hard carbon (HC) electrodes at high C-rates, the use of different conductive additives was explored. In this context, multiwalled carbon nanotubes (CNTs) supplied by UpCatalyst (figure 4e) were employed and evaluated as a partial replacement for carbon black Super C45 (mass proportion combination CNT:C45 1:1). This conductive mixture was combined with the acid pretreated HC in sample OP\_X\_4\_B2C. As second alternative approach to enhance the performance of HCs at high C-rates involved ball milling of HCs that had previously undergone acid pretreatment and a complete carbonization protocol. The milling was performed in a planetary mill equipped with zirconia jars and balls ( $\varnothing = 15\text{ mm}$ ), using eight cycles of 30 minutes each at 550 rpm. As a result, the carbon particle size was reduced to the  $0.6\text{--}1.2\text{ }\mu\text{m}$  range (Figure 4c and 4d). The resulting carbon, combined with a conductive additive blend (C45:CNT), was evaluated as sample OP\_X\_4BM\_B2C. Additionally, a second batch of hard carbons was synthesized following the same alternative methodologies, with the sole modification of adjusting the final carbonization temperature to  $850\text{ }^{\circ}\text{C}$  in the third stage of the protocol. This procedure yielded the samples OP\_X\_1\_C (acid-pretreated), OP\_X\_1\_B2C (C45:CNT conductive additive mixture), and OP\_X\_1BM\_B2C (ball-milled hard carbon). Figure 4f presents the Raman spectra of the hard carbon samples and the UpCatalyst CNTs. All samples exhibited the characteristic D and G bands of carbonaceous materials, located at  $\sim 1347\text{ cm}^{-1}$  and  $\sim 1595\text{ cm}^{-1}$  for the hard carbons. The broader FWHM of the D band relative to the G band indicates a predominantly amorphous character or a high defect density in the carbon structure. Following the OP modifications (acid pretreatment and ball milling), both a narrowing of the peaks and a decrease in the ID/IG ratio were observed, suggesting a reduction in defect density and the possible development of graphitic domains. In the case of CNTs, the D and G bands appeared at  $\sim 1345\text{ cm}^{-1}$  and  $\sim 1574\text{ cm}^{-1}$ , respectively, along with an additional D' band at  $\sim 1602\text{ cm}^{-1}$ , confirming their highly ordered graphitic structure.

To perform the electrochemical tests, the tape-casting technique was employed to fabricate electrodes from the previously described HC samples. An aqueous slurry with 76 wt% liquid content was prepared. The solid fraction of the slurry (24 wt%) consisted of HC as the active material (90 wt%), Super C45 carbon black as the conductive additive (5 wt% for

samples OP, OP\_X\_4\_C, and OP\_X\_1\_C), or a mixture of C45 and CNTs from UpCatalyst (2.5 wt% each for samples OP\_X\_4\_B2C, OP\_X\_4BM\_B2C, OP\_X\_1\_B2C, and OP\_X\_1BM\_B2C). Carboxymethyl cellulose (CMC, 5 wt%) was used as the binder. The solid and liquid components were placed in the jar of a vibratory mill (SPEX) together with 25 stainless steel balls ( $\varnothing = 2$  mm) and mixed for 20 min, resulting in a homogeneous slurry. Using a doctor blade, the slurry was cast onto etched aluminum foil at wet thicknesses between 150 and 200  $\mu\text{m}$ . The drying procedure consisted of an initial step at room temperature for 6 h, followed by vacuum drying at 80  $^{\circ}\text{C}$  for 16 h. For slurries prepared from ball-milled carbons, the slurry formulation had to be modified due to bubble formation and cracking during drying. The bubble issue was mitigated by adjusting the slurry pH with NaOH, added to deionized water in a proportion of 0.5 wt% relative to the HC content. Cracking was resolved by incorporating styrene-butadiene rubber (SBR) as an additional binder, combined with CMC in a ratio of SBR (2 wt%) to CMC (3 wt%). After solving these issues, electrodes ( $\varnothing = 12$  mm) were punched, with mass loadings between 2 and 3  $\text{mg}\cdot\text{cm}^{-2}$ . Finally, they were vacuum-dried at 120  $^{\circ}\text{C}$  overnight before being assembled into cells for electrochemical testing.

Three-electrode Swagelok (SW) cells in half-cell configuration were used to carry out electrochemical tests by means of galvanostatic charge–discharge. The working electrode consisted of the previously described HC-based electrodes, while sodium discs ( $\varnothing = 12$  mm) were employed as both counter and reference electrodes. Cell assembly was conducted in a glovebox under controlled atmosphere ( $\text{O}_2/\text{H}_2\text{O}$ ), using glass fiber separators (Whatman GF/D) and 1 M  $\text{NaPF}_6$  in EC:PC (E-lyte VP1007) as electrolyte. Galvanostatic charge–discharge tests were performed using a Biologic VMP3 potentiostat within the potential range of 0.002–2 V versus  $\text{Na}^+/\text{Na}$ . Cycling was conducted at different C-rates, beginning with 5 cycles at C/15 relative to the theoretical capacity of carbon ( $\sim 372$   $\text{mA}\cdot\text{h}\cdot\text{g}^{-1}$ ), followed by sets of 5 cycles at C/10, C/5, C/2, C, 2C, 5C, and 10C (equivalent to current densities from 0.025 to 3.72  $\text{A}\cdot\text{g}^{-1}$ ). Figure 5 presents the corresponding charge–discharge profiles together with coulombic efficiency and rate capability plots for all tested samples. For all carbons except those subjected to ball milling, the profiles exhibited a sloping region between  $\sim 1$  V and  $\sim 0.15$  V at C-rates below C, which was slightly more pronounced in capacity for samples carbonized at 850  $^{\circ}\text{C}$  ( $\sim 110$   $\text{mA}\cdot\text{h}\cdot\text{g}^{-1}$ ).

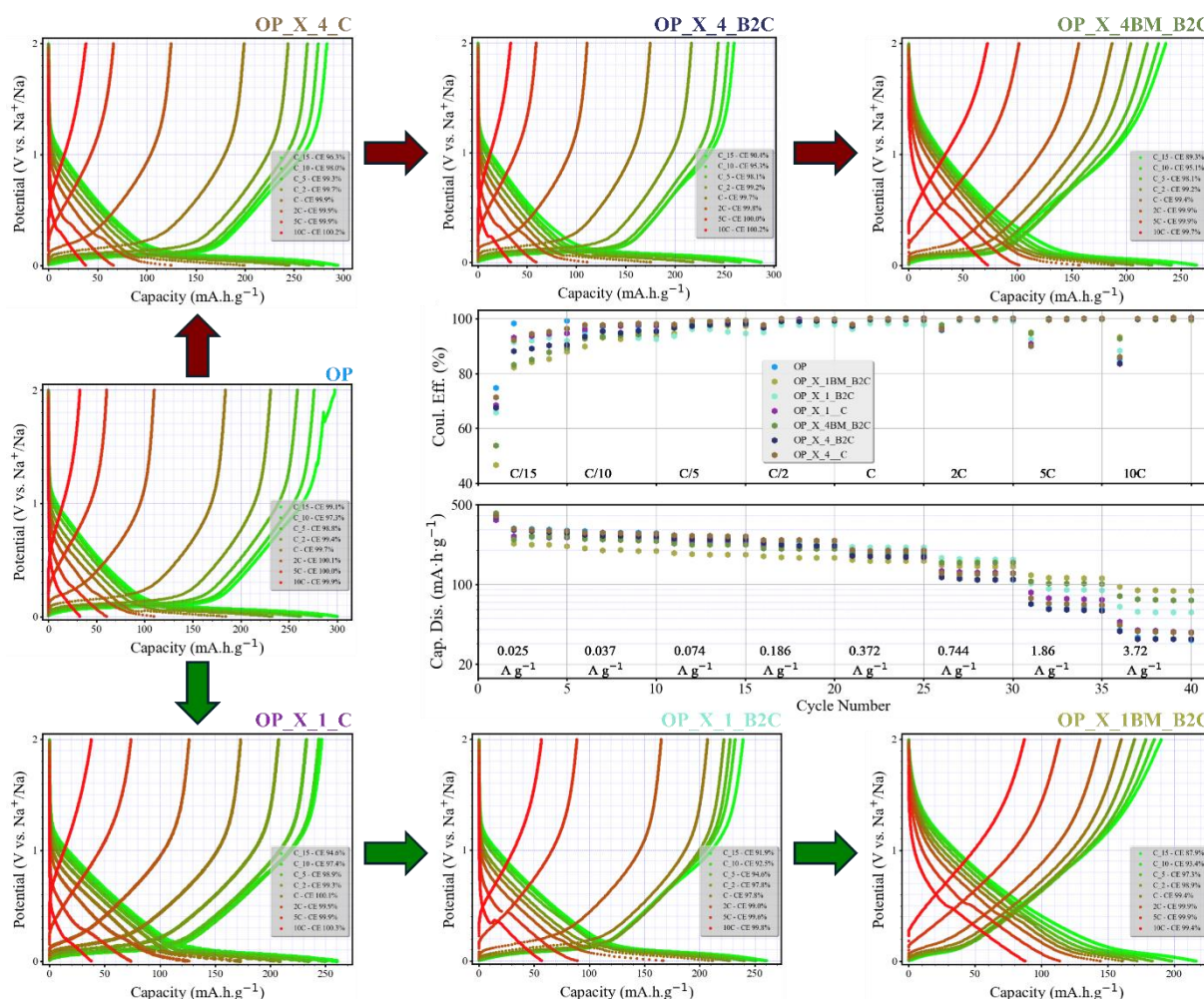


**Figure 5.** Biowaste derived Hard carbons: Charge-Discharge profiles at different C-rates. Electrochemical performance, (middle up) Coulombic efficiency and (middle down) Rate capability.

In contrast, carbons carbonized at 1050 °C displayed an extended plateau region between  $\sim 0.15$  V and  $\sim 0.002$  V, reaching  $\sim 200$  mA $\cdot$ h $\cdot$ g<sup>-1</sup>. Ball-milled samples exhibited considerably broader sloping regions ( $\sim 1.35$ – $0.2$  V), which suppressed the contribution of the plateau, an effect particularly evident for carbons treated at 850 °C. At low C-rates ( $<C$ ), non-ball-milled samples delivered higher capacities; however, as the plateau contribution diminished and eventually disappeared with increasing current, samples with reduced particle size achieved higher capacities. A clear trend is observed whereby smaller particle sizes lead to lower initial coulombic efficiency (ICE) values (Table 6).

**Table 6.** Characteristics of hard carbons derived from biowaste.

Sample ID	Precursor	Protocol of carbonization	Comments (HCl pretreatment /CNT /ball milling)	Capacity @ 1C (mA·h/g)	Capacity @ 5C (mA·h/g)	ICE (%)
OP	Olive pits	120°C(30min) 500°C(30min) 1050°C(12h)	no/no/no	187.2	61.7	74.8
OP_X_4_C	Olive pits	120°C(30min) 500°C(30min) 1050°C(12h)	yes/no/no	198.7	66.8	71.3
OP_X_4_B2C	Olive pits	120°C(30min) 500°C(30min) 1050°C(12h)	yes/yes/no	175.8	59.7	67.5
OP_X_4BM_B2C	Olive pits	120°C(30min) 500°C(30min) 1050°C(12h)	yes/yes/yes	188.1	102.1	53.8
OP_X_1_C	Olive pits	120°C(30min) 500°C(30min) 850°C(12h)	yes/no/no	175.6	75.5	68.4
OP_X_1_B2C	Olive pits	120°C(30min) 500°C(30min) 850°C(12h)	yes/yes/no	211.6	90.1	65.8
OP_X_1BM_B2C	Olive pits	120°C(30min) 500°C(30min) 850°C(12h)	yes/yes/yes	161.4	114.3	46.7

**Xylose derived HC's:** A 0.5 M aqueous solution of xylose was prepared and subjected to hydrothermal carbonization at 190 °C for 6 h. Following the treatment, the xylose remained largely in solution, and centrifugation yielded only a minor amount of solid sediment. The supernatant was subsequently dried in an oven at 100 °C for 3 h and then at 70 °C for 2 days, resulting in a viscous residue of low mass. These results indicate that, in the absence of a catalyst, hydrothermal treatment of xylose is not effective for carbon material production. To address the low efficiency of the hydrothermal process, HCl (2 mL per gram of xylose) was added as a catalyst, which increased the mass yield. The resulting hydrothermal product, after washing, filtration, and drying, was subjected to the same carbonization protocol used for the olive pit-derived hard carbons, with the addition of a final step at 1400 °C under argon. This produced the carbon shown in Figure 6a (sample Xyl 1). Electrodes prepared according to the previously described protocol, with mass loadings of 2–3 mg·cm<sup>-2</sup>, were tested in identical cell configurations and cycling conditions as the olive pit carbons. The galvanostatic profiles of Xyl 1 (Figure 6d) exhibited a short slope (~0.85–0.2 V, <80 mA·h·g<sup>-1</sup>) followed by an extended plateau (~220 mA·h·g<sup>-1</sup>), which disappeared at C-rates above C/2, leading to a sharp capacity drop. To enhance high-rate performance, the acid content during the hydrothermal step was increased to 4 mL per gram of xylose, producing the carbon shown in Figure 6b (sample Xyl 2). SEM analysis revealed a marked reduction in particle size. The corresponding charge–discharge profiles (Figure 6e) displayed a slightly extended slope region (~1.05–0.2 V, <85



$\text{mA}\cdot\text{h}\cdot\text{g}^{-1}$ ) and a reduced plateau ( $\sim 190 \text{ mA}\cdot\text{h}\cdot\text{g}^{-1}$ ) that remained stable up to  $\text{C-rate} = \text{C}$ . Finally, further increasing the acid content to 8 mL per gram of xylose and limiting the carbonization temperature to 900 °C yielded the carbon shown in Figure 6c (sample Xyl 3), characterized by even smaller particles. The galvanostatic profiles of Xyl 3 (figure 6f) exhibited a significantly extended slope region and a pronounced reduction of the plateau, even at low C-rates.

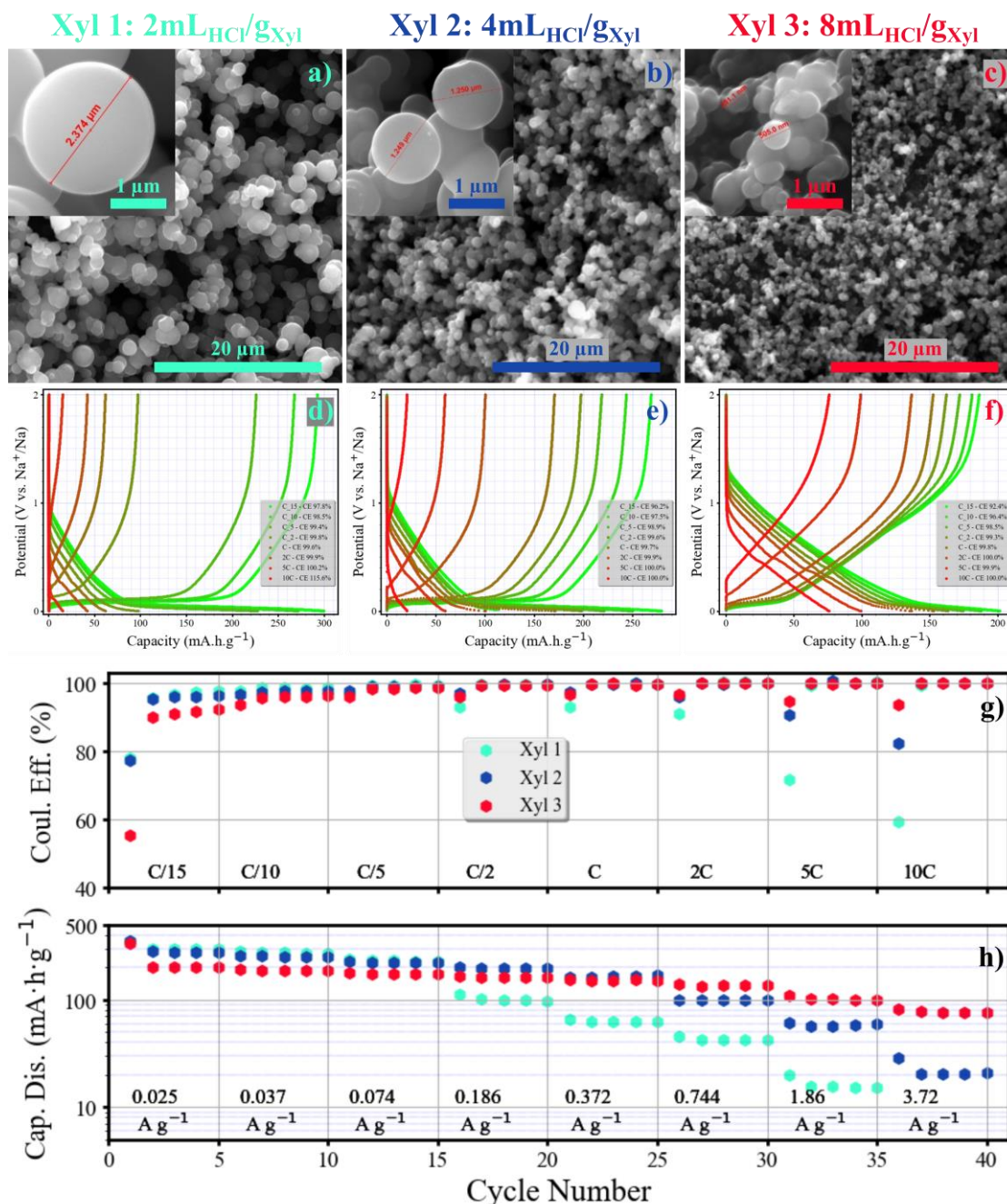


**Figure 6.** Hard carbons derived from Xylose: Scanning electron microscopy (SEM) images at 2000x magnification (inset: 32000x magnification), (a) Xyl 1 ,(b) Xyl 2 and (c) Xyl 3. Charge-Discharge profiles at different C-rates, (d) Xyl 1 ,(e) Xyl 2 and (f) Xyl 3. Electrochemical performance, (g) Coulombic efficiency and (h) Rate capability.

**Table 7.** Features of some hard carbons derived from xylose.

Sample ID	Precursor	Protocol of carbonization	Average particle size ( $\mu\text{m}$ )	Capacity @ 1C (mA·h/g)	Capacity @ 5C (mA·h/g)	ICE (%)
Xyl 1	Xylose	120°C(30min) 500°C(30min) 1400°C(12h)	1.8 - 2.6	62.3	15.6	77.9
Xyl 2	Xylose	120°C(30min) 500°C(30min) 1400°C(12h)	0.8 - 1.3	164.8	58.4	77.2
Xyl 3	Xylose	120°C(30min) 500°C(30min) 900°C(12h)	0.4 - 0.8	153.1	100.5	55.2

### 2.1.2.3. Carbon fibers

The driving idea of this work was the possibility to use recycled carbons rather than having to synthesize new ones for the negative electrode of sodium-ion capacitors. Preliminary results provided during the submission of the proposal tended to indicate that recycled carbon fibers issued from carbon based composite material could be an innovative solution to address this issue. Subsequently, the recycled carbon fibers investigated in the MUSIC project were obtained from the recycling of carbon fabrics/epoxy resin composites by different processes, namely pyrolysis (Apply carbon Cie), solvolysis (ExtratHive Cie) and vapothermolysis (AlphaRecyclage Composites Cie). Pitch based carbon fibers and PAN-based carbon fibers were obtained from these 3 different recycling processes and were compared to raw carbon fibers from the same precursors.

Recycled carbon fibers were delivered as entangled fibers, one to ten centimeters long. Such length was much too large for the preparation of carbon suspension (ink) for tape casting electrodes of sodium-ion capacitors. This issue was solved by the use of ball-milling process which consisted in milling at 400 rpm the carbon fibers using RETSCH Planetary Mill PM 100. The fibers were milled in a tungsten carbide (WC) jar filled with 85 WC beads of 7mm diameter. Micrometer size carbon fibers were obtained with such milling process. The fibers were investigated from a structural/microstructural and chemical point of view at different stages of their manufacturing process.

The crystallinity of the carbon fibers was investigated using Raman spectroscopy. The Raman spectra display two prominent peaks located at approximately  $1365\text{ cm}^{-1}$  and  $1590\text{ cm}^{-1}$ , corresponding to the D and G bands, respectively. The D band is associated with disordered carbon structures, while the G band reflects the presence of graphitic ( $\text{sp}^2$ -hybridized) carbon domains. The intensity ratio of the D to G bands,  $R=\text{ID}/\text{IG}$ , is plotted in Figure 7a. For the PAN-derived carbon fibers, this ratio is approximately 0.9, suggesting a nearly balanced contribution of graphitized and amorphous carbon. This substantial presence of structural disorder is particularly advantageous for anode applications, as amorphous carbon domains promote porosity, which can enhance sodium storage capacity.

In comparison, pitch-based carbon fibers exhibit significantly lower ID/IG ratio, typically ranging from 0.3 to 0.5, indicative of a more graphitized structure. These results demonstrate that recycling processes tend to increase disorder in highly graphitized carbon materials, whereas partially graphitized PAN-based fibers retain their structural characteristics. These findings suggest that PAN-based carbon fibers possess more favorable characteristics for sodium-ion insertion compared to their pitch-based counterparts. Thus, vapothermolysis and pyrolysis of the PAN-based carbon fibers were chosen for further investigations. In order to be processed as tape-casted electrodes they were further ball-milled for several milling time in order to decrease the particle size as demonstrated in Fig. 7b. Concomitantly, the specific surface area measured by BET increases (Fig. 7c) while reaching a plateau after 4 hours milling time. However, it was difficult to process electrodes out of the ball-milled material for more than 2 hours (results from two different partners CICE and CNRS-IMN).

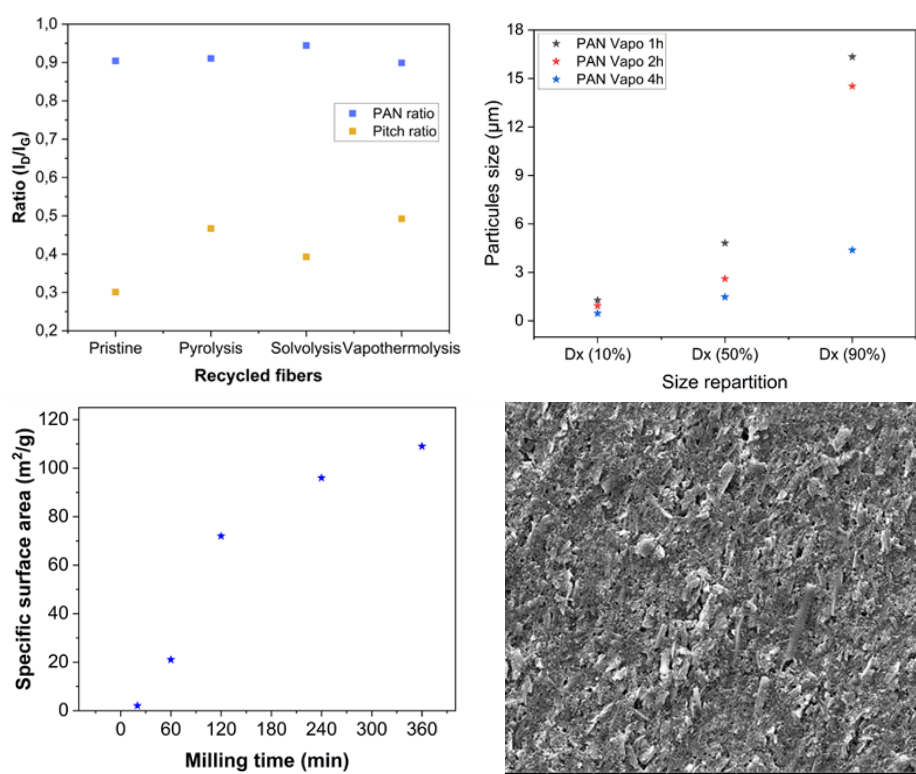


**Figure 7.** a) Raman Spectra of PAN and Pitch-based carbon fibers recycled by different recycling processes and the ratio of the amorphous and graphitic carbon in the carbon fibers; b) particle size distribution of PAN-based carbon fibers recycled by vapothermolysis after different ball-milling times; c) specific surface vs milling time at 400 rpm for PAN carbon fibers recycled by vapothermolysis; d) electrode surface for a 1 hour ball-milling time of PAN-based carbon fibers recycled by vapothermolysis.

Subsequently, electrodes were prepared out of the most promising recycled carbon fibers and compared to standard hard carbon negative electrode (HC). Electrodes were prepared by formulating an ink. A carbon fiber-based electrode ink was formulated with a solvent-

to-solid ratio of 70 wt.% water and 30 wt.% solid components. The solid fraction comprised 90 wt.% carbon fibers, 5 wt.% carboxymethyl cellulose (CMC) as a binder, and 5 wt.% carbon black (C-ENERGY™ Super C45) as a conductive additive. The ink was cast onto etched aluminum foil using an automatic film applicator (doctor blade) from Captair®. The coated foil was left to dry for 2 hours at room temperature, followed by overnight drying at 60 °C in a ventilated oven. Electrode disks with a diameter of 12 mm were then punched from the dried films for subsequent electrochemical testing (Fig. 7d).

For electrochemical measurements, Swagelok-type half-cells were assembled for sodium-ion electrochemical insertion studies, using recycled carbon fiber electrodes as the working electrode and a circular piece of metallic sodium serving as both counter and reference electrode. The electrolyte consisted of 300  $\mu\text{L}$  of 1 M  $\text{NaPF}_6$  dissolved in a 1:1 (v/v) mixture of ethylene carbonate (EC) and propylene carbonate (PC), supplied by E-lyte. The electrolyte was used to impregnate two glass microfiber separators (Whatman). All experiments were performed in a temperature-controlled environment maintained at 22 °C.

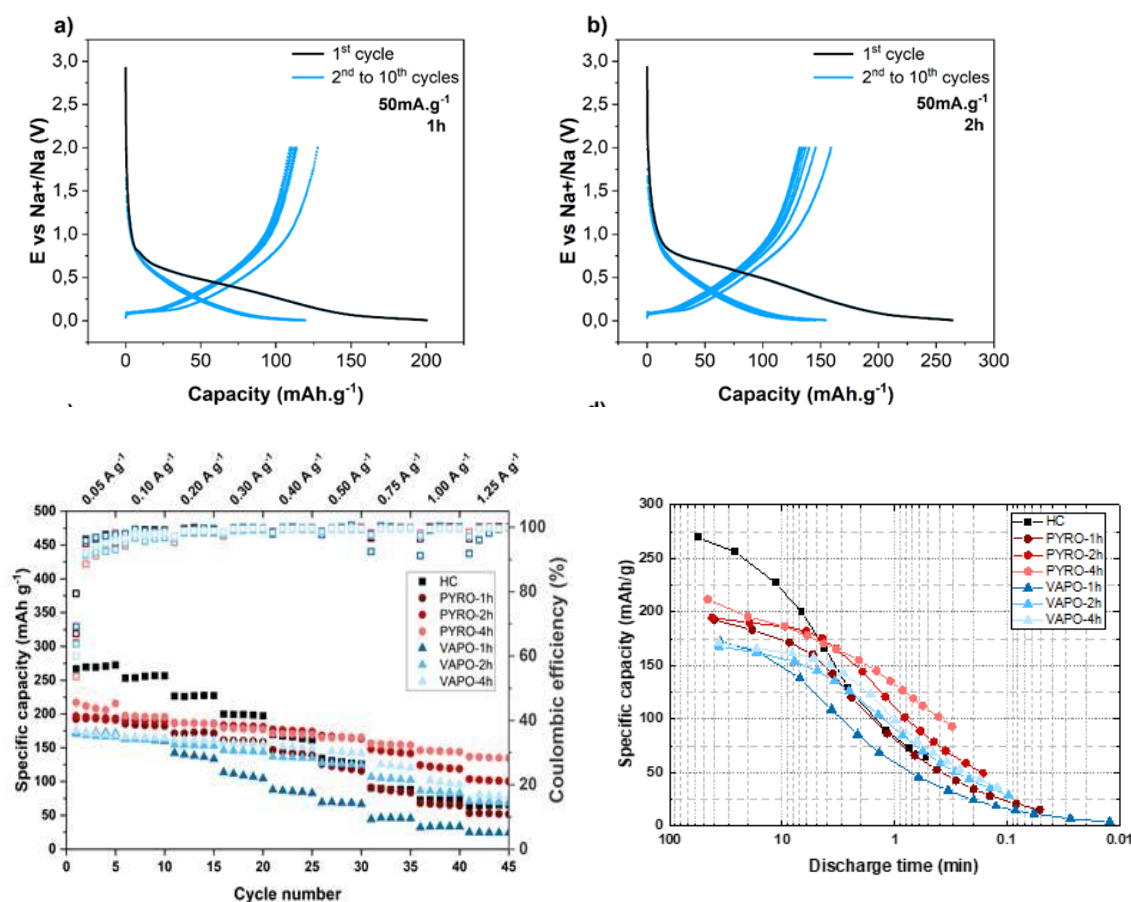


**Figure 8.** Discharge-charge profiles at 50 mA.g<sup>-1</sup> of PAN carbon fibers recycled by vapo-thermolysis a) milled 2h and b) milled 4h; c) specific charge/discharge capacity vs current density for different PAN-based carbon fibers recycled with vapo-thermolysis and pyrolysis processes, compared to standard hard carbon negative electrode (HC, black



plot); d) specific capacity vs discharge time for different PAN-based carbon fibers recycled with vapothermolysis and pyrolysis processes, compared to standard hard carbon negative electrode.

The GCPL capacity profiles for recycled carbon fibers exhibit similarities to those of hard carbon. This comparison allows for the extrapolation of sodium storage mechanisms in carbon fiber electrodes. As shown in Figure 8a and b, a sloping region between 1.0 and 0.2 V is observed, which is typically associated with the pseudo-capacitive insertion of sodium ions into both the open pores of the carbon material. Between 0.2 V and 0.005 V, the profile exhibits a short sloppy region that approaches a plateau. This differs from the expected profile for hard carbon, which typically features a longer plateau region, highlighting the contribution of sodium intercalation into the graphitic layers, akin to lithium intercalation.

At low charge/discharge rates ( $0.05 \text{ A}\cdot\text{g}^{-1}$ , corresponding to  $\sim 5.5$  hours per cycle, Fig. 8c), the recycled carbon fiber electrodes did not achieve the same specific capacity as the hard carbon reference. However, at higher rates ( $1 \text{ A}\cdot\text{g}^{-1}$ ,  $\sim 6$ -minute cycles), the PAN-based recycled carbon fibers exhibited superior performance, demonstrating higher specific capacity than the hard carbon. This enhanced performance at high charge/discharge rates is particularly advantageous for sodium-ion capacitor applications, where rapid energy delivery is critical (Fig. 8d). The lower rate capability of hard carbon, which stores charge predominantly through pseudocapacitive mechanisms, limits the overall device speed. Among the recycled fibers, those obtained via pyrolysis exhibited the best performance, outperforming those recycled through vapothermolysis and HC at fast charging/discharging rates.

## 2.2 Advanced Electrolytes

The state-of-the-art electrolyte for sodium-ion based energy storage systems is 1 M  $\text{NaPF}_6$  in EC:PC (1:1 by weight). Within the project we are aiming to find alternative electrolytes which display high conductivity ( $> 10 \text{ mS cm}^{-1}$ ), wide electrochemical stability window ( $> 5 \text{ V}$ ) and reduced fluorine content (compared to  $\text{NaPF}_6$ ) that can operate beyond  $70^\circ\text{C}$  (KPR7). For this purpose, a wide range of different electrolytes was investigated, changing the conducting salt from  $\text{NaPF}_6$  to less fluorinated alternatives, namely NaTFSI, NaFSI and NaDFOB. Also, solvent alternatives such as TEG and GVL have been studied. In order to increase the ESW additives (FEC and NaDFOB) have been employed.

Firstly, the SoA electrolyte was produced by E-lyte and delivered to the project partners (Table 8). Within the project, various new electrolyte formulations have been agreed upon

which were also provided by E-lyte and are included in the table. Conductivity values for selected electrolytes, conducted by E-lyte, are shown in Table 9.

**Table 8.** Electrolyte formulations provided by E-lyte to different partners.

Partner	Formulation	Amount
HIU/KIT	1M NaPF <sub>6</sub> in EC:PC 1:1 (by weight)	250 g (5 x 50g)
University Jena	1M NaPF <sub>6</sub> in EC:PC 1:1 (by weight)	250 g (5 x 50g)
CICE	1M NaPF <sub>6</sub> in EC:PC 1:1 (by weight)	50g x4
CNRS-IMN	1M NaPF <sub>6</sub> in EC:PC 1:1 (by weight)	250 g (5 x 50g)
IRTJV	1M NaPF <sub>6</sub> in EC:PC 1:1 (by weight)	250 g (5 x 50g)
Beyonder	1M NaPF <sub>6</sub> in EC:PC 1:1 (by weight)	50 g
CIRIMAT	1M NaPF <sub>6</sub> in EC:PC 1:1 (by weight)	250 g (5 x 50g)
FSU Jena	1M NaTFSI EC:PC (1:1) (by weight)	10 g
	1M NaFSI EC:PC (1:1) (by weight)	10 g
	1M NaTFSI EC:PC (1:1) (by weight) + 2 wt% FEC	10 g
	1M NaTFSI EC:PC (1:1) (by weight) + 2 wt% NaDFOB	10g
	1M NaPF <sub>6</sub> TEG:PC (3:7) (by weight) + 2 wt% FEC	10g
	NaDFOB	2 g
	2x 12g 1 M NaTFSI in TEG (1,1,2,2,-Tetraethoxyethane):PC (30:70, by wt.%)	10 g
CICE	2x 12g 1 M NaTFSI in TEG (1,1,2,2,-Tetraethoxyethane):PC (30:70, by wt.%) + 2wt.% FEC	10 g
	1M NaPF <sub>6</sub> in EC:PC 1:1 (by weight)	50g x4
CNRS-IMN	1M NaPF <sub>6</sub> in EC:PC 1:1 (by weight)	50g x2
CIRIMAT /UPS	1M NaPF <sub>6</sub> in EC:PC 1:1 (by weight)	50g x2
FSU Jena	1M NaTFSI in EC:PC (1:1) by weight	25 g
	1M NaFSI in EC:PC (1:1) by weight	25 g
	1M NaPF <sub>6</sub> in PEC:TEG (1,1,2,2,-Tetraethoxyethane) (7:3) by weight	25 g
	1M NaTFSI in EC:PC (1:1) by weight + 2wt.% NaBOB	25 g
	1M NaTFSI in PEC:TEG (7:3) by weight + 2wt.%NaBOB	25 g
	1M NaPF <sub>6</sub> in PEC:TEG (7:3) by weight + 2wt.%NaBOB	25 g
CICE	1M NaPF <sub>6</sub> in EC:PC 1:1 (by weight)	50g x4
	1M NaClO <sub>4</sub> in EC:PC 1:1 (by weight)	25g x2
CIRIMAT /UPS	1M NaPF <sub>6</sub> in EC:PC 1:1 (by weight)	2 x 50 g
Beyonder	1M NaPF <sub>6</sub> in EC:PC 1:1 (by weight)	10 x 50 g
CRIMAT / UPS	1M NaPF <sub>6</sub> in EC:PC 1:1 (by weight)	4 x 50
HIU / KIT	1M NaPF <sub>6</sub> in EC:PC 1:1 (by weight)	2 x 50 g
CICE	1M NaPF <sub>6</sub> in EC:PC 1:1 (by weight)	2 x 50 g
FSU Jena	1 M NaTFSI in EC:PC (by weight)	25 g
	1 M NaTFSI in EC:PC (by weight) + 2 wt.% FEC	25 g
	1 M NaTFSI in EC:PC (by weight) + 2 wt.% NaDFOB	25 g

Partner	Formulation	Amount
	1 M NaTFSI in EC:PC (by weight) + 2 wt.% FEC + 2wt.% NaDFOB	10 g
	1M NaFSI EC:PC (1:1) (by weight)	25 g
UP Catalyst	1M NaPF <sub>6</sub> in EC:PC 1:1 (by weight)	0.05 kg x 1
CICE	1M NaPF <sub>6</sub> in EC:PC 1:1 (by weight)	0.05 kg x 10
HIU / KIT	1M NaPF <sub>6</sub> in EC:PC 1:1 (by weight)	0.05 kg x 2
FSU Jena	NaBoB	0.02 kg
	1 M NaFSI in EC:PC 1:1 (by weight) + 2wt% FEC + 2wt% NaDFOB	0.05 kg x 4
	1 M NaFSI in EC:GVL 1:1 (by weight) + 2wt% FEC + 2wt% NaDFOB (mit GVL= $\gamma$ -Valerolactone)	0.05 kg x 4
	1 M NaFSI in DMC:EC 1:1 (by weight) + 2wt% FEC + 2wt% NaDFOB	0.05 kg x 4
	1 M NaFSI in DEC:EC 1:1 (by weight) + 2wt% FEC + 2wt% NaDFOB	0.05 kg x 4
CNRS-IMN	1M NaPF <sub>6</sub> in EC:PC 1:1 (by weight)	0.05kg x 4

**Table 9.** Conductivity values of selected electrolyte formulations measured by E-lyte.

No.	Electrolyte formulation	Conductivity $\sigma$ (mS/cm) @ 25 °C*
1	1M NaTFSI in EC:PC (1:1) by weight	6.48
2	1 M NaFSI in EC:PC (1:1) by weight	8.63
3	1 M NaPF <sub>6</sub> in EC:PC (1:1) by weight	8.16
4	1 M NaPF <sub>6</sub> in PC:TEG (7:3) by weight	4.63
5	1 M NaTFSI in EC:PC (1:1) by weight + 2wt.% FEC	6.38
6	1 M NaTFSI in EC:PC (1:1) by weight + 2wt.% NaDFOB	6.00
7	1 M NaTFSI in EC:PC (1:1) by weight + 2wt.% FEC + 2wt.% NaDFOB	5.94
8	1 M NaPF <sub>6</sub> in PC:TEG (7:3) by weight + 2wt.% FEC	4.60
9	1 M NaFSI in EC : PC (50 : 50, by wt.) + 2 wt.% FEC + 2 wt.% NaDFOB	8.36
10	1 M NaFSI in EC : GVL (50 : 50, by wt.) + 2 wt.% FEC + 2 wt.% NaDFOB	9.55
11	1 M NaFSI in DMC : EC (50 : 50, by wt.) + 2 wt.% FEC + 2 wt.% NaDFOB	12.57
12	1 M NaFSI in DEC : EC (50 : 50, by wt.) + 2 wt.% FEC + 2 wt.% NaDFOB	8.55

\*The results correlated with the first one of the single point conductivity measurement @ 25°C

## 3 Discussion and Conclusions

### 3.1 Advanced Electrode materials

#### 3.1.1 Modified High Specific Surface Area Activated Carbons

Nitric acid treatment was chosen as a straightforward and gentle method to modify the textural properties and surface chemistry of activated carbons. This treatment altered the carbon's characteristics: the specific surface area increased, and the pore size distribution shifted toward narrower pores.

Simultaneously, enriching the carbon surface with oxygen yielded both positive and negative outcomes. On the positive side, it led to increased overall stability against oxidation at higher potentials and an improved capacitance near the point of zero charge. Conversely, the narrower pores restricted electrolyte adsorption and slowed the rate response of the positive electrode. While some oxygen-rich surface functional groups can aid electrolyte transport or stability at more positive potentials, others might be prone to decomposition within the typical electrochemical stability window.

At this stage of development, this treatment is considered a promising first step. Further refinement is needed, especially through an additional high-temperature treatment. This would aim to create more oxidation-resistant functional groups and ensure a more accessible pore volume.

#### 3.1.2 Soft carbon from PVC precursors

PVC precursor was chosen to synthesize waste-derived SC. Since the particle size is critical for a good performance at high rates, an optimization process was carried out where the particle size was reduced from 20 to an optimum size of 2  $\mu\text{m}$ . The ball milling process was performed as an intermediate step instead of a final step to avoid a large surface degradation (the final calcination step was used to heal the surface as well as its main purpose of carbon calcination). This optimization resulted in a soft carbon with an ICE of 77% and first charge capacity of 226 mAh/g at C/15 rate, retaining 104 mAh/g at 1C. These results, together with additional optimization work will lead to a publication.

#### 3.1.3 Hard carbons

Hard carbons were synthesized from biowaste using olive pits as the precursor. The initial carbonization protocol yielded materials with poor performance at C-rates above C/2, which motivated the application of an acid pretreatment to modify the raw structure. Further optimization included particle-size reduction via ball milling (exposing closed pores, increasing surface area, and reducing interparticle spacing), adjustment of the

carbonization temperature (controlling graphitic domain size), and partial replacement of the conductive additive with CNTs (enhancing contact between the conductive network and the active material). The resulting optimized electrode, despite a low ICE, exhibited the best electrochemical performance at high C-rates (Table 6), attributable to the reduction of closed pores and the increased effective surface area facilitating sodium insertion/extraction.

In parallel, carbons were synthesized from xylose, where particle size was tuned by controlled HCl addition during the hydrothermal step and by moderating the carbonization temperature. Low-particle-size xylose-derived carbons yielded electrodes with low ICE but improved electrochemical performance at high C-rates (Table 7).

#### **3.1.4 Recycled CNFs**

Carbon-based composite materials are an increasing part of new aircrafts, thus replacing aluminium parts for achieving lower weight. However, end of life for these composites is a main challenge for aircraft manufacturers. Tons of carbon-based composites are buried in the ground every year, due to the lack of regulation at the European level for recycling these materials. Composite material parts from components reaching end-of-life are not the only ones that will need a solution for recycling in the medium term. Current forming processes generate significant production waste, non-compliant parts, and so forth, adding more to the volume needing recycling in the short term.

Within the framework of the MUSIC project, we have demonstrated that carbon fibers issued from recycling processes can be implemented as efficient negative electrodes in sodium-ion capacitors with improved power performances compared to standard hard carbon electrodes. Moreover, the origin of the recycled carbon fibers and the most interesting recycling processes have been identified in order to prepare electrodes that can compete with existing materials. The impressive sources of recycled carbon fibers are coping well with the expectations of large scale manufacturing of sodium-ion capacitors.

Currently, large batches of PAN-based recycled carbon fibers have been provided by composites recycling companies in order to investigate the scaling-up of such electrodes and their performance in larger sodium-ion cells. Their interactions with pre-sodiation sacrificial molecules is also to be investigated in order to point out differences with standard hard carbon electrodes.

### 3.2 Advanced Electrolytes

The state-of-the-art electrolyte 1 M NaPF<sub>6</sub> in EC:PC (1:1 by weight) was firstly defined as Gen0, produced and then delivered by E-lyte to various project partners. In the following, a wide electrolyte matrix was investigated in order to optimize performance, sustainability and safety of the final electrolyte configuration. This work has already led to the publication of one paper, three more are currently under preparation. The investigation of the novel electrolytes is ongoing and the results will be discussed in detail in the future deliverable D3.4 (M40).

## 4 Recommendation

Numerous carbonaceous active materials and electrolyte formulations have been developed and optimized in the first 30 months of the MUSIC project. Some of them show very promising properties (gravimetric capacity, coulombic efficiency, rate capability, stability, etc.) compared with the benchmarking components at the lab cell level.

However, some work is still needed to evaluate the combination of some of the best-performing components (anode, cathode and electrolyte) within the same device and in a larger format cell, as well as their integration with the sacrificial salts also developed within the WP3, required for the in-situ anode pre-sodiation step.

## 5 Risk register

**Table 10.** Risk Register.

Risk No.	What is the risk	Probability of risk occurrence <sup>1</sup>	Effect of risk <sup>2</sup>	Solutions to overcome the risk
<b>WP3.1</b>	Reproducibility issues associated to the bio-wastes.	Medium	Medium	Preconditioning steps to homogenize the properties and performance of derived carbons.

<sup>1</sup> Probability risk will occur: 1 = high, 2 = medium, 3 = low

<sup>2</sup> Effect when risk occurs: 1 = high, 2 = medium, 3 = low

## 6 Acknowledgement

The authors would like to thank the partners in the project for their valuable comments on previous drafts and for performing the review.

### Project partners

**Table 11.** Project Partners.

#	PARTICIPANT SHORT NAME	PARTNER ORGANISATION NAME	COUNTRY
1	CICE	CENTRO DE INVESTIGACION COOPERATIVA DE ENERGIAS ALTERNATIVAS FUNDACION, CIC ENERGIGUNE FUNDAZIOA	Spain
2	EUR	CLANCY HAUSSLER RITA	Austria
3	KIT	KARLSRUHER INSTITUT FUER TECHNOLOGIE	Germany
4	CNRS	CENTRE NATIONAL DE LA RECHERCHE SCIENTIFIQUE CNRS	France
4.1	IMN	NANTES UNIVERSITE (Affiliated)	France
5	UPS	UNIVERSITE PAUL SABATIER TOULOUSE III	France
6	FSU	FRIEDRICH-SCHILLER-UNIVERSITAT JENA	Germany
7	IRT-JV	INSTITUT DE RECHERCHE TECHNOLOGIQUE JULES VERNE	France
8	ELY	E-LYTE INNOVATIONS GMBH	Germany
9	BYD	BEYONDER AS	Norway
10	BCARE	BATTERYCARE S. L.	Spain
12	TALGO	PATENTES TALGO SL	Spain
13	UPC	UP CATALYST	Estonia



This project has received funding from the European Union's Horizon Europe programme for research and innovation under grant agreement No. 101092080. This document reflects the views of the author and does not reflect the views of the European Commission. While every effort has been made to ensure the accuracy and completeness of this document, the European Commission cannot be held responsible for errors or omissions, whatever their cause.